Publications of the Astronomical Society of the Pacific, **119**: 1163–1178, 2007 October

Toward More Precise Survey Photometry for PanSTARRS and LSST: Measuring Directly the Optical Transmission Spectrum of the Atmosphere

Christopher W. Stubbs, F. William High, Matthew R. George, Kimberly L. DeRose, and Stéphane Blondin

Department of Physics and Harvard-Smithsonian Center for Astrophysics, Harvard University, Cambridge, MA

John L. Tonry, Kenneth C. Chambers, and Benjamin R. Granett

Institute for Astronomy, University of Hawaii, Honolulu, HI

David L. Burke

Kavli Institute for Particle Astrophysics and Cosmology, Stanford Linear Accelerator Center, Palo Alto, CA

and

R. Chris Smith

Cerro Tololo Inter-American Observatory/National Optical Astronomy Observatory, Tucson, AZ

Received 2007 June 26; accepted 2007 August 7; published 2007 October 31

ABSTRACT. Motivated by the recognition that variation in the optical transmission of the atmosphere is probably the main limitation to the precision of ground-based CCD measurements of celestial fluxes, we review the physical processes that attenuate the passage of light through Earth's atmosphere. The next generation of astronomical surveys, such as PanSTARRS and LSST, will greatly benefit from dedicated apparatus to obtain atmospheric transmission data that can be associated with each survey image. We review and compare various approaches to this measurement problem, including photometry, spectroscopy, and LIDAR. In conjunction with careful measurements of instrumental throughput, atmospheric transmission measurements should allow next-generation imaging surveys to produce photometry of unprecedented precision. Our primary concerns are the real-time determination of aerosol scattering and absorption by water along the line of sight, both of which can vary over the course of a night's observations.

Online material: color figures

1. INTRODUCTION

Careful CCD measurements of differential photometry, i.e., comparing fluxes from similar stars in the same image, allow comparisons at the millimagnitude level (Hartman et al. 2005; Everett & Howell 2001). On the other hand, with considerable effort the Sloan Digital Sky Survey (SDSS) achieved (Padmanabhan et al. 2007) of order 1% uncertainty in zero-point uniformity across the sky in the g, r, i, and z bands, and twice that in u.

What accounts for this apparent factor of 10 difference in our ability to compare the fluxes of celestial objects? The SDSS team attributes (Padmanabhan et al. 2007) the dominant contribution to their zero-point uncertainty as arising from "… unmodelled atmospheric variations …" By combining 58 scans across one SDSS equatorial region, Ivezić et al. (2007) achieved zero-point scatter of just under 1%. This falls short of the $\sqrt{58} \sim 7$ fold improvement over single-scan calibration that one would expect from random errors. This implies that the SDSS photometry is bottoming out in some combination of flat-fielding residuals and atmospheric variability. This fact does not diminish the importance or the power of the SDSS data set, but future survey programs need to identify and overcome the factors that limited the precision of the SDSS photometry if they wish to do better.

When comparing celestial fluxes from objects in a common image, only the *angular* variation in atmospheric transmission, across the angular separation between objects, can introduce errors due to differences in atmospheric transmission. On the other hand, comparing fluxes from survey images taken at different times and through different air masses is susceptible to both temporal and line-of-sight changes in atmospheric transmission. In our view this difference accounts for the discrepancy in precision between differential photometry *within* one image and establishing a common photometric zero point *across* different survey images.

This simple fact indicts variations in atmospheric transmission as imposing the major limitation to the precision of ground-based CCD photometry from all-sky surveys. Disentangling source brightness, instrumental response, and variable atmospheric transmission is challenging. Multiple visits to each field, ideally with different instrument orientations, are certainly

helpful, along with careful attention to flat-fielding and suppression of instrumental artifacts.

High-precision *differential* photometry does achieve the Poisson limit. Numerous examples of this have been presented, and we summarize a few salient points from these studies. Everett & Howell (2001) performed aperture photometry on carefully flat-fielded images and demonstrated that by comparing fluxes to a robust ensemble average of flux from sources within 0.25°, they could achieve Poisson-limited performance. Hartman et al. (2005) used image subtraction techniques and demonstrated differential photometry with scatter below 1 mmag. Enhanced dynamic range high-precision photometry was carried out by Tonry et al. (2005) using an orthogonal transfer CCD. These successes all indicate that flat-fielding can be done at the millimagnitude level and that Poisson-limited photometry is a worthwhile goal. Achieving uniform zero points across the surveyed region of the sky amounts to making a high-precision set of measurements. The survey accuracy, i.e., knowing with certainty the corresponding fluxes in joules s^{-1} m^{-2}, is far less important (for nearly all astronomical applications) than attaining good precision.

The opportunity for achieving high-precision photometric measurements in upcoming multiband sky surveys such as the Panoramic Survey Telescope and Rapid Response System (PanSTARRS; Kaiser et al. 2002) and the Large Synoptic Survey Telescope (LSST)[1] motivates a comprehensive assessment of the limitations of ground-based CCD photometry. Stubbs & Tonry (2006) provide a framework for this appraisal, and that paper suggests factoring the problem into (1) characterizing the wavelength dependence of the response of the telescope, optics, and instrument and (2) determining the optical transmission properties of the atmosphere. This paper deals with the issue of understanding and measuring the optical transmission of the atmosphere.

Our eventual goal is to produce the spectrum of atmospheric optical transmission through which the observation occurred, for each cataloged object flux from each image in the survey archive. In conjunction with detailed knowledge of instrumental sensitivity versus wavelength, we can then (at least in principle) perform synthetic photometry with trial spectral energy distributions (SEDs) for all sources and compare these spectral integrations with the number of counts actually detected. This "forward modeling" approach has been recently described for the infrared by Bailey et al. (2007). In essence, we advocate using the same techniques that are being applied to correcting for atmospheric absorption in spectrophotometry (e.g., Bessell 1999; Stritzinger et al. 2005) and spectroscopy (e.g., Hadrava 2006) to broadband imaging data. By reporting the survey fluxes as measured in the "natural system" of each detector on the focal plane, along with the appropriate instrumental and atmospheric transmission profiles, we can construct an atmosphere-corrected flux for each object of interest using one or more trial SEDs. This avoids having to specify color terms for the detectors, which are intrinsically intermingled with the assumed spectrum of the source of interest. It also addresses the problem of second-order "color–air mass" extinction corrections. Users who are satisfied with the more standard treatment are, of course, still free to apply a global approximation to instrumental color terms and atmospheric extinction corrections. Knowledge of the actual optical transmission function for each measurement could also play a role in more precise *K*-corrections for supernovae (Miknaitis et al. 2007).

It is interesting to note that in the era just before the advent of CCDs, photoelectric photometrists were pushing toward millimagnitude photometry. In this context we draw particular attention to the remarkable paper by Young and collaborators (Young et al. 1991), that raises many of the issues that we address here. It would appear that the advent of CCD detectors stalled this initiative. Now that CCD performance and flat-fielding techniques have advanced, it is time to revisit the issues that stand between the current state of the art and the fundamental limit imposed by Poisson statistics.

One important difference between our philosophy and that described in Young et al. (1991) is that those authors considered a single photometric instrument for both atmospheric characterization and celestial flux measurements, whereas we intend to evaluate the optimal choice of *dedicated* instrumentation for atmospheric characterization. Given the choice between using their allocated telescope time either to fully characterize atmospheric extinction or to observe their program objects, most astronomers have opted for the latter. The SDSS project did include a separate "Photometric Monitoring Telescope" that was equipped with nominally the same filter set as the 2.5 m survey telescope, but filter passband and detector quantum efficiency (QE) differences between the main survey system and the monitoring telescope gave rise to color terms that prevented this approach from reaching its full potential (Tucker et al. 2006).

The Pierre Auger Observatory measures Cerenkov light from high-energy cosmic-ray showers in the atmosphere. Molecules and aerosols scatter and absorb this signal on the path to the detectors. Proper interpretation of the detected light requires a knowledge of the optical properties of the atmosphere, and this has led the team to establish a sophisticated set of instruments, including LIDAR and photometric monitors to measure the aerosol content and scattering properties of the local atmosphere (BenZvi et al. 2007a, 2007b).

The photometric calibration plans for PanSTARRS (Magnier 2007) and LSST (Burke et al. 2006) both include apparatus dedicated to the determination of atmospheric extinction, to allow the wide-field survey imagers to focus on science images of the sky without needing to allocate time to atmospheric characterization.

The question then becomes, What is the best method to determine atmospheric extinction, using dedicated apparatus

[1] See LSST Science Case, http://www.lsst.org/Science/lsst_baseline.shtml.

that runs in conjunction with a broadband all-sky survey, and what cadence of observations is needed to capture the temporal and directional variations in extinction?

1.1. Some Formalism

The total photon flux [$S(t)$, photons per second] that we detect from some celestial source is an integral over wavelength,

$$S(t) = A \int \mathcal{F}(\lambda,t)T(\lambda,\hat{z},t)I(\lambda,t)\, d\lambda, \quad (1)$$

where the $\mathcal{F}$ is the spectral photon distributions (SPDs; evaluated above the atmosphere) of the sky and all sources present, $I(\lambda,t)$ is the dimensionless instrumental transmission, including optics, filter, and detector, A is the effective collecting area of the system, and $T(\lambda,\hat{z},t)$ is the wavelength-dependent atmospheric transmission along the direction $\hat{z}$ at the time t of the measurement, averaged over the exposure time. [We adopt the convention here that the units of $\mathcal{F}$ are photons $\mathrm{nm}^{-1}\ \mathrm{s}^{-1}\ \mathrm{m}^{-2}$, derived from the conventional spectral energy distribution as $\mathcal{F} = F_\lambda\lambda/(hc)$.]

We have described elsewhere (Stubbs et al. 2007) a program of measuring explicitly $I(\lambda,t)$, the wavelength dependence of the instrumental response. Our focus in this paper is the determination of $T(\lambda,\hat{z},t)$, the time-dependent and line-of-sight–dependent optical transmission of the atmosphere.

The claim that observing conditions are "photometric" during a night amounts to assuming that $T(\lambda,\hat{z},t) = T(\lambda,\theta_{\mathrm{zen}})$, i.e., time independent and axisymmetric, depending only on zenith angle. Furthermore, the typical corrections for atmospheric extinction assume a simple dependence in which all magnitudes are corrected by a band-specific extinction coefficient k that is multiplied by the secant of the zenith angle. The extinction coefficient for each passband is taken as a universal number, independent of the source's spectrum. As shown below, these standard photometric approximations will fail to produce the accuracy that we propose to attain. Furthermore, the regression of all magnitudes to zero air mass (above the atmosphere) introduces a strong leverage on any uncertainty in the extinction coefficients, as we are extrapolating into a regime that is not directly observable from the ground.

Wade & Horne (1988) present a useful formulation of atmospheric transmission, which we generalize to make clear the distinct processes at work, and any potential time dependence. At any wavelength the optical transmission of the atmosphere can be represented as

$$T(\lambda,\hat{z},t) = \exp\left[-\sum_i \tau_i(\lambda,t,\hat{z})\chi^{\alpha_i}(\hat{z})\right], \quad (2)$$

where τ_i is the optical depth (at one air mass) for each attenuation process, χ is the air mass along the line of sight with unit vector $\hat{z}$, and α_i is the air-mass dependence of the attenuation process. For spectral regions where the attenuation processes are unsaturated we would expect $\alpha_{\mathrm{unsat}} = 1$, whereas for saturated lines we would expect the absorption from the wings of the line to scale with $\alpha_{\mathrm{sat}} = 0.5$. Atmospheric water has numerous narrow molecular absorption features; some are saturated and some are not. Wade & Horne (1988) suggest that this produces an effective $\alpha_{\mathrm{water}} = 0.6$. We should expect similar behavior from other complex molecular absorption band structures.

The direct determination of each component of atmospheric attenuation, ideally co-boresighted and simultaneous with the survey imager, would help address our currently inadequate correction for the atmosphere. Our goal in this paper is to explore alternative approaches to this measurement problem and to suggest measurements that would help illuminate a shrewd choice of technology.

Measurements of the optical transmission properties of the atmosphere can exploit either natural celestial sources to backlight the atmosphere, or man-made illumination, which is observed through backscatter. (Albert et al. [2006] have undertaken a program to use ground-based observations of artificial sources on satellites, but we do not explore that option in this paper.)

The resulting atmospheric transmission measurements can then be used in isolation or in conjunction with detailed computer models such as MODTRAN (Anderson et al. 2001). We suggest that it makes sense to fully exploit the comprehensive knowledge of atmospheric physics that has been incorporated into these sophisticated codes.

In the sections that follow we review the physics of optical transmission through the atmosphere, and then we discuss in turn merits of spectroscopic, photometric, and light detection and ranging (LIDAR) measurements for characterizing extinction. We then describe how the combination of atmospheric transmission functions and computer modeling could be exploited in a forward modeling approach to astronomical photometry, and we close with a suggested set of next steps.

2. ATTENUATION BY THE ATMOSPHERE AT OPTICAL WAVELENGTHS, AND ITS VARIABILITY

2.1. The Final Four for a Photon: Rayleigh Scattering, Molecular Absorption, Aerosols, and Clouds

As light propagates to us from celestial sources it experiences numerous opportunities to interact with material. Extinction at the source, through the Galaxy, and in other intervening regions can all play a role in distorting the spectrum. From the standpoint of this paper, these astrophysical processes can be either sources of information or a nuisance, and we do not address them here. Our concern is the astrophysically uninteresting attenuation from the final four hurdles faced by an astronomical photon: scattering and absorption from atoms and molecules

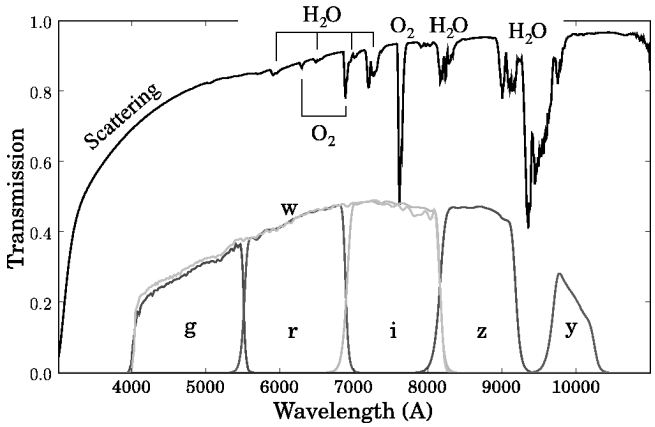

FIG. 1.—Photon transmission through one air mass, with PanSTARRS instrumental sensitivity. This plot shows the different contributions to attenuation of light in passing through the atmosphere, along with filter bands times the expected detector QE, for PanSTARRS. The LSST filter set is similar, but also includes a *u* band. The atmospheric transmission was computed with MODTRAN for one air mass at an elevation of 10,000 ft (305 m), with an initial spectral resolution of 1 cm^{-1}, boxcar smoothed to 1 nm. [*See the electronic edition of PASP for a color version of this figure.*]

in the atmosphere, scattering from suspended aerosols, and extinction due to clouds.

Figure 1 shows the expected attenuation of flux due to the atmosphere, alongside the filter passbands for the PanSTARRS survey, and illustrates where the different components of extinction will afflict our measurements.

Table 1 provides an estimate of the integrated attenuation that we expect within each survey passband, from the different components of atmospheric attenuation. This calculation presumes a source that has a photon spectrum $\mathcal{F}(\lambda) \propto \lambda^0$, which for our spectral region of interest approximately corresponds to a blackbody of 4500 K. We integrated the different components of $T(\lambda)$ separately in order to gain some intuition about the relative importance of scattering versus absorption.

The next step is to assess how different source spectra behave as they propagate through the atmosphere and the instrumental response function. Since it is awkward to obtain high-precision spectrophotometric data in the attenuated spectral regions of interest, we used theoretical models of stellar spectra for computing the effects of the atmosphere. We used the theoretical spectra from Kurucz (1993) to compute the flux attenuation due to the atmosphere by performing synthetic photometry across the different $I(\lambda)$ system response functions that we expect for PanSTARRS. We obtained Kurucz's modeled stellar spectra from the astronomical catalog portion of the Catalog Database System.[2] These STScI stellar atlas data are $F_\lambda(\lambda)$ tabulations, which we converted into photon spectral distributions $\mathcal{F}(\lambda) = F_\lambda\lambda$, with an arbitrary common multiplicative normalization.

[2] See http://www.stsci.edu/hst/observatory/cdbs/astronomical_catalogs.html.

TABLE 1
ESTIMATED TRANSMISSION AT ONE AIR MASS FROM THE SMOOTHLY VARYING COMPONENTS (RAYLEIGH SCATTERING AND AEROSOLS) AND ABSORPTION FROM MOLECULAR LINES, FOR THE PANSTARRS SYSTEM

Band	T_{smooth}	T_{lines}	Total
PanSTARRS *g*	0.815	1.000	0.815
PanSTARRS *r*	0.894	0.996	0.890
PanSTARRS *i*	0.949	0.961	0.912
PanSTARRS *z*	0.964	0.970	0.935
PanSTARRS *y*	0.961	0.947	0.910

NOTES.—Note that the air-mass dependence, α, of these can be quite different. We have included the anticipated effects of two Al reflections, of filter transmission, and of detector QE in the system's response functions. These numbers presume a source with a constant photon flux per nanometer. The effects of molecular absorption and aerosols are comparable for *i*, *z*, and *y*.

Using a spectral resolution of $\Delta\lambda = 0.1$ nm we integrated the source spectra shown in Table 2 through the transmission function that corresponds to $\chi = 1$ air mass. The *error* that would be incurred by making the usual assumption that the extinction (in magnitudes) scales linearly in air mass for all attenuation processes is roughly 0.01, 0.02, and 0.03 mag per air mass in the *r*, *i*, and *z* bands, respectively.

We drew two conclusions from this exercise: (1) we cannot ignore the interplay between extinction and the source spectrum, and (2) we need to properly account for the different air-mass scaling for line absorption versus scattering.

A number of studies have explored the stability of extinction at astronomical sites, including Krisciunas et al. (1987), Reimann et al. (1992), Frogel (1998), Schuster et al. (2002), de Vaucouleurs & Angione (1973), and Tucker et al. (2006). There are numerous reasons to expect variability in atmospheric extinction. We should expect a variation in aerosol and water content with the direction of prevailing winds and with local meteorology. The solar "weather" influences the ozone fraction

TABLE 2
CALCULATED EXTINCTION COEFFICIENTS FOR PANSTARRS PASSBANDS, FOR DIFFERENT ASTRONOMICAL OBJECTS

Source	k_g	k_r	k_i	k_z	k_y
O5 V	0.23	0.13	0.08	0.06	0.07
B5 V	0.23	0.13	0.08	0.06	0.07
A3 V	0.23	0.13	0.08	0.06	0.07
F5 V	0.22	0.12	0.08	0.06	0.07
G3 V	0.21	0.12	0.08	0.06	0.07
K4 V	0.20	0.12	0.08	0.06	0.07
M2 V	0.20	0.12	0.08	0.06	0.07

NOTES.—The first column lists the template spectrum used; the subsequent columns list the computed extinction coefficient, in magnitudes per air mass. The interplay between color and extinction is most pronounced in the bluer bands. The difference in spectral weighting accounts for the difference between these values and those of the previous table.

in the upper atmosphere. Some of these dependencies are nontrivial. One such example is the apparent dependence (Pakstiene 2001; Reimann et al. 1992; Roosen & Angione 1977) of extinction on absolute humidity, even in bluer spectral regions that are well away from H_2O line absorption, allegedly due to water absorption by aerosols changing their sizes and hence their scattering properties. The dependence of extinction on meteorology, and over time, has been explored by Reimann et al. (1992), Frogel (1998), and Pakstiene (2001).

Table 3 shows a summary of weather statistics for a 4 yr period at Cerro Tololo Inter-American Observatory (CTIO). We take these values as being representative of weather variability at good astronomical sites around the world. The data were obtained from the SOAR Telescope online archive.[3]

TABLE 3
SUMMARY OF WEATHER AT CTIO, 2001 JANUARY 1 TO 2005 JANUARY 2

Parameter	10th	25th	50th	75th	90th
Temperature (C)	6.7	11.9	15.2	17.4	18.9
Pressure (mbar)	781	782	784	785	786
Relative humidity (%)	8	13	23	38	55
Wind direction (deg)	32	60	107	238	313
Wind speed (m s^{-1})	0.675	1.62	3.195	5.85	8.595

NOTES.—The table lists percentiles for the distribution of the relevant meteorological parameter. We make the conservative assumption that the time actually spent observing follows this overall pattern.

2.2. Molecular Scattering

Elastic scattering (Rayleigh 1899) from atoms and molecules in the air has a cross section that varies as $\sigma_{\rm Ray}(\lambda) \sim \lambda^{-4}$, with a slight correction that arises from wavelength dependence of the index of refraction. Hansen & Travis (1974) give the optical depth (at zenith) for Rayleigh scattering to be

$$\tau_{\rm Ray} = 0.008569\lambda^{-4}(1 + 0.0113\lambda^{-2} + 0.00013\lambda^{-4}) \times\left(\frac{P}{1013.25\ \text{mbar}}\right),$$

where λ is in microns. This process dominates over inelastic scattering, such that the inelastic contribution to attenuation is negligible.

The attenuation due to Rayleigh scattering thus depends on the pressure of the atmosphere along the line of sight. Barometric pressure varies with a typical timescale of days and will fluctuate as high- and low-pressure systems pass over an observatory. This changes the effective air mass along a fixed line of sight, in proportion to the pressure fluctuation. A measurement taken at CTIO at an air mass χ under a pressure that is δP different from the nominal $P_0 = 784$ nm will suffer a change in transmission of $\delta T_{\rm Ray} = 6 \times 10^{-3}\chi(\delta P/P_0)(1\ \mu\text{m}/\lambda)^4$. A variation in attenuation of <1 mmag therefore requires $\delta T_{\rm Ray} < 0.001$ or $\chi(\delta P/P_0)(1\ \mu\text{m}/\lambda)^4 < 0.17$. Using the 90th percentile pressure excursion for CTIO, an *uncorrected* Rayleigh extinction perturbation under 1 mmag at $\lambda = 500$ nm, in the *g* band, corresponds to restricting $\chi < 2.6$ air masses during a large pressure excursion.

It is however very tractable to calculate how changes in local barometric pressure would introduce an air mass–dependent shift in the Rayleigh transmission. Millimagnitude photometry will require a pressure-dependent correction to attenuation from Rayleigh scattering only for very blue bands observed at air masses around $\chi \sim 3$. We are also fortunate that conditions with very low barometric pressure are often accompanied by weather that precludes opening the dome. The Rayleigh scattering should be axisymmetric about the zenith with a time dependence driven only by pressure variations. The characteristic spectral dependence and spatial symmetry of extinction by molecular scattering can be combined with independent measurements of barometric pressure and air mass to provide precise determination of extinction due to this process, subject to observational confirmation.

2.3. Aerosols

Scattering from aerosols and particulates in the atmosphere is in the awkward "Mie" regime where the particulate size is comparable to the wavelength. This gives rise to a cross section $\sigma_{\rm Mie}(\lambda) \sim \lambda^k$, where k depends on the size and shape distributions of the scattering particles. Since aerosol scattering is in the optically thin regime for all wavelengths, we expect an air-mass exponent of $\alpha_{\rm aero} = 1$. Sinyuk et al. (2007) claim that most aerosols reside within ~4 km of the Earth's surface.

There is ample evidence for volcanic eruptions producing long-term change in the optical transmission of the atmosphere. These global events have more local counterparts, due to changes in wind direction, to regional forest fires, to lofted marine salts, etc. This implies that the transmission spectrum $T_{\rm aero}(\lambda,\hat{z},t)$ will have both time dependence and azimuth dependence.

Holben et al. (2001) present data for both atmospheric water content and the optical depth due to aerosols, obtained from the AERONET system, at Mauna Loa. We strongly suspect that this is a good proxy for the aerosol characteristics that we expect on Haleakala, where PanSTARRS-1 is situated. The AERONET instrument measures the scattering of solar radiation as a function of angle away from the Sun, in multiple bands. Although the observations in the different bands are not strictly simultaneous, the cycle time through the filter set is only 8 s. They report values of optical depth τ for $\lambda = 340$, 380, 440, 500, 675, 870, 940, and 1020 nm. They use the 940 nm channel for measuring water content, by comparing the solar flux seen there to that of adjacent bands.

The AERONET Level 2 data have been selected to avoid days with obvious clouds, and the data are processed in order

[3] See archive at http://www.soartelescope.org/release/02about/eng_about/weather/main_weather.html.

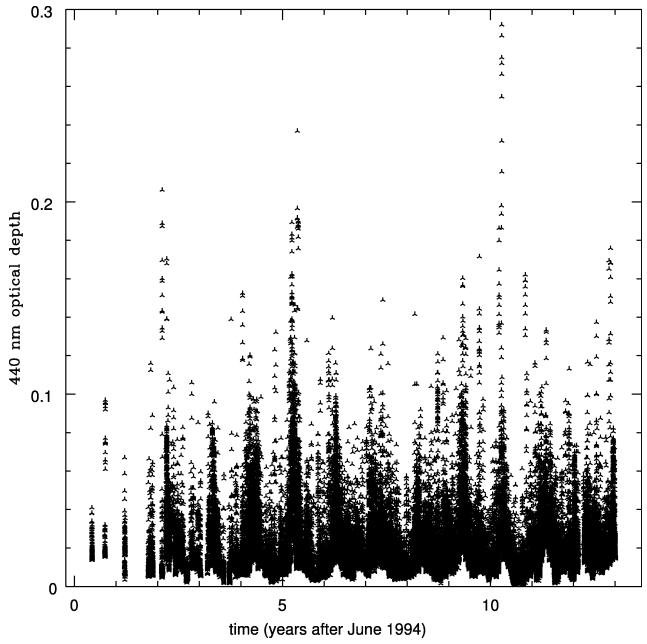

FIG. 2.—Aerosol optical depth. The graph shows the daytime aerosol optical depth at 440 nm over time as reported from solar flux measurements by the AERONET system on Mauna Loa, near the site of the PanSTARRS-1 system. The vertical axis is optical depth τ, where a fraction $e^{-\tau}$ is transmitted through one air mass. Time is in years after 1994 June. There is clear evidence for seasonal cycles, as well as considerable variation on short timescales.

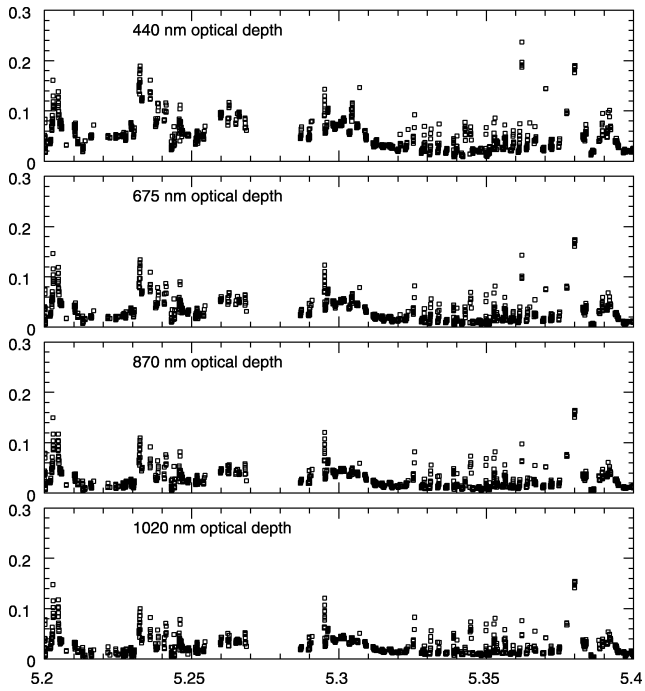

FIG. 3.—Aerosol optical depths at different wavelengths. This plot shows in more detail the AERONET reported daytime Mauna Loa aerosol optical depth at different wavelengths vs. time. The plots span a period of 72 days. Note the variation in spectral dependence of the attenuation spikes.

to extract the various components of attenuation, as described in Holben et al. (2001). In the descriptions that follow we used the Level 2.0 AERONET data, obtained from the AERONET Web site.[4]

Figure 2 shows a 15 yr record of aerosol optical depth at Mauna Loa, at 440 nm. Figure 3 is an expanded view of a period spanning 0.2 yr and shows the aerosol optical depth fluctuations at 1020, 870, 675, and 440 nm. Figures 4 and 5 show that different "extinction spikes" have different spectral character. Some extinction spikes are changes in transparency, with little wavelength dependence, while others clearly exhibit more attenuation at the shorter wavelengths. Figure 6 shows the cumulative aerosol optical depth distributions for the period of time shown in Figure 2. The median aerosol optical depth values at 1020, 440, and 340 nm are 0.007, 0.015, and 0.018, respectively. Figure 7 shows the cumulative distribution of variation in the AERONET aerosol optical depth measurements.

Measuring the extinction due to aerosols is one of our main challenges. It may be that daytime measurements, of the kind reported by Holben et al. (2001), could be used to estimate nighttime aerosol scattering, but we need to explore the extent to which this is true. Most aerosols are low in the atmosphere. This, together with the observed short-term variation in aerosol optical depth, implies that we should expect azimuth dependence of the aerosol transmission across the sky.

[4] See http://aeronet.gsfc.nasa.gov/new_web/data.html.

2.4. Molecular Absorption

Absorption features in the spectra of atmospheric constituents produce a complex set of absorption bands and features. Ozone, water, O_2, and OH molecules all contribute to this absorption. In fact, the atmosphere is essentially opaque in numerous narrow regions, especially for $\lambda > 740$ nm. A high spectral resolution determination of the molecular atmospheric absorption above Kitt Peak National Observatory is presented in Hinkle et al. (2003).

2.4.1. Oxygen

The strong absorption features at 690 and 760 nm due to O_2, the "B" and "A" bands in the nomenclature of Fraunhofer, are stable over time, since they depend on the integrated oxygen content along the line of sight. The same arguments given above about the pressure dependence of Rayleigh scattering apply here as well. We therefore expect this component of atmospheric transmission, T_{O_2}, to be axisymmetric about the zenith and stable over time, again with a slight pressure dependence.

This picture is borne out by inspecting the corrections applied to spectrophotometric data by Bessell (1999). Figures 1 and 2

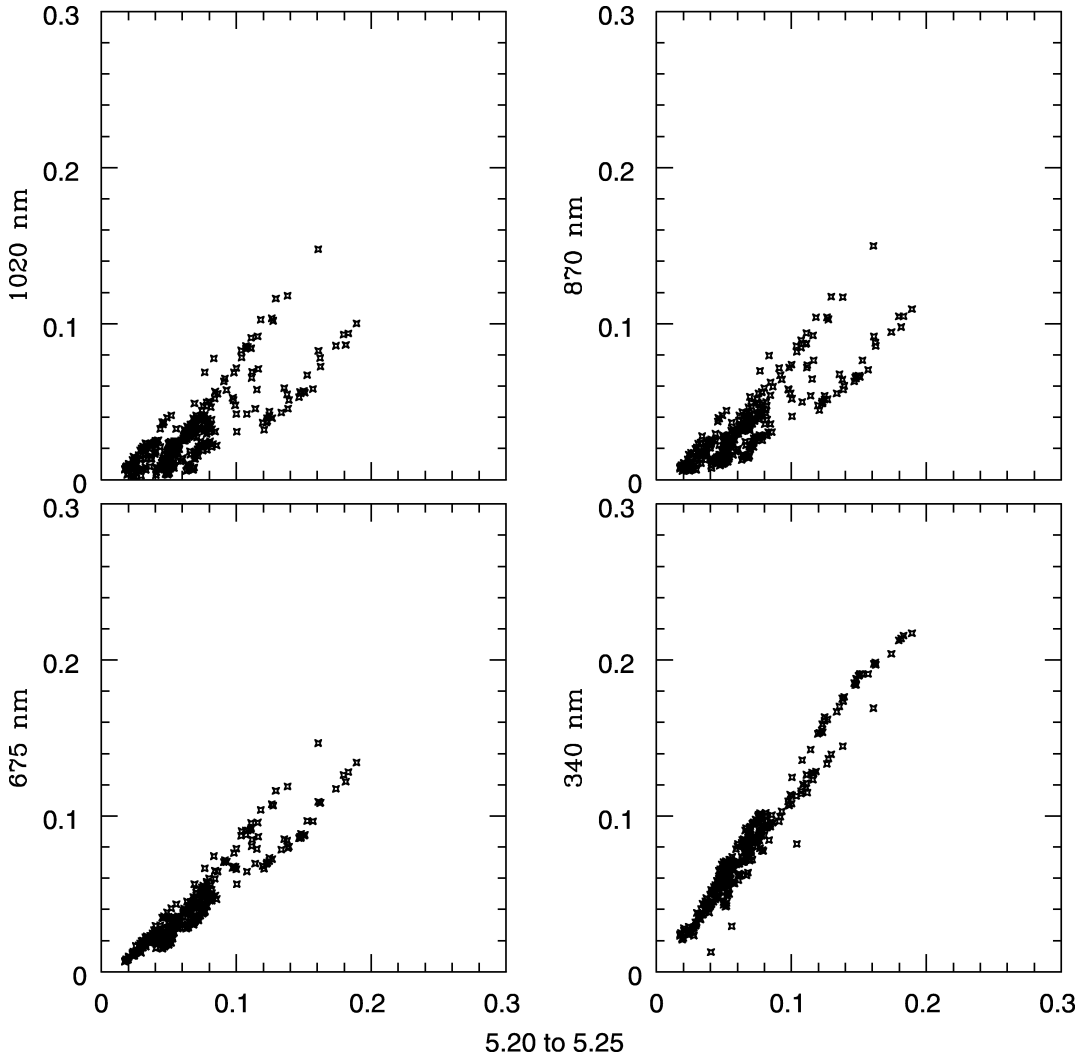

FIG. 4.—Extinction excursion. These panels show the Mauna Loa AERONET attenuation at 1020 nm (*upper left*), 870 nm (*upper right*), 675 nm (*lower left*), and 340 nm (*lower right*) plotted vs. the attenuation at 440 nm, for the period between 5.20 and 5.25 yr of Fig. 2. A wavelength-independent change in transparency would generate a line with a slope of $m = +1$ in each of the panels. Aerosol scattering would have slopes less than unity in all except the lower right panel. The data show evidence for both kinds of excursions in this time period.

of that paper clearly show much smaller residuals in the A and B bands as compared to water absorption regions.

2.4.2. Ozone

The opacity of ozone is responsible for the total loss of atmospheric transmission below 300 nm. The Chappuis band of ozone influences transmission for $500\ \text{nm} < \lambda < 700\ \text{nm}$, with an attenuation of a few percent at 600 nm. The measurement of ozone in the atmosphere is of great interest due to its important role in the Earth's radiation balance and climate change. This has led to the development and deployment of sophisticated space-based instruments that are optimized for the determination of the ozone content of the atmosphere. These data sets can be used to determine the ozone above observatories. Satellite measurements of the ozone content versus time over Hilo, HI, are shown in Figure 8. These illustrative data were obtained from the Total Ozone Mapping Spectrometer (TOMS) instrument (Jaross et al. 2003) on board the *Earth Probe* satellite, and we obtained the data for Figure 8 from the TOMS Web site.[5]

The determination of ozone content in the atmosphere above the observatories can be obtained from satellite remote sensing data with sufficient accuracy and temporal resolution for our purposes. Since the attenuation due to ozone is only a few

[5] See http://toms.gsfc.nasa.gov/eptoms/ep_ovplist_a.html.

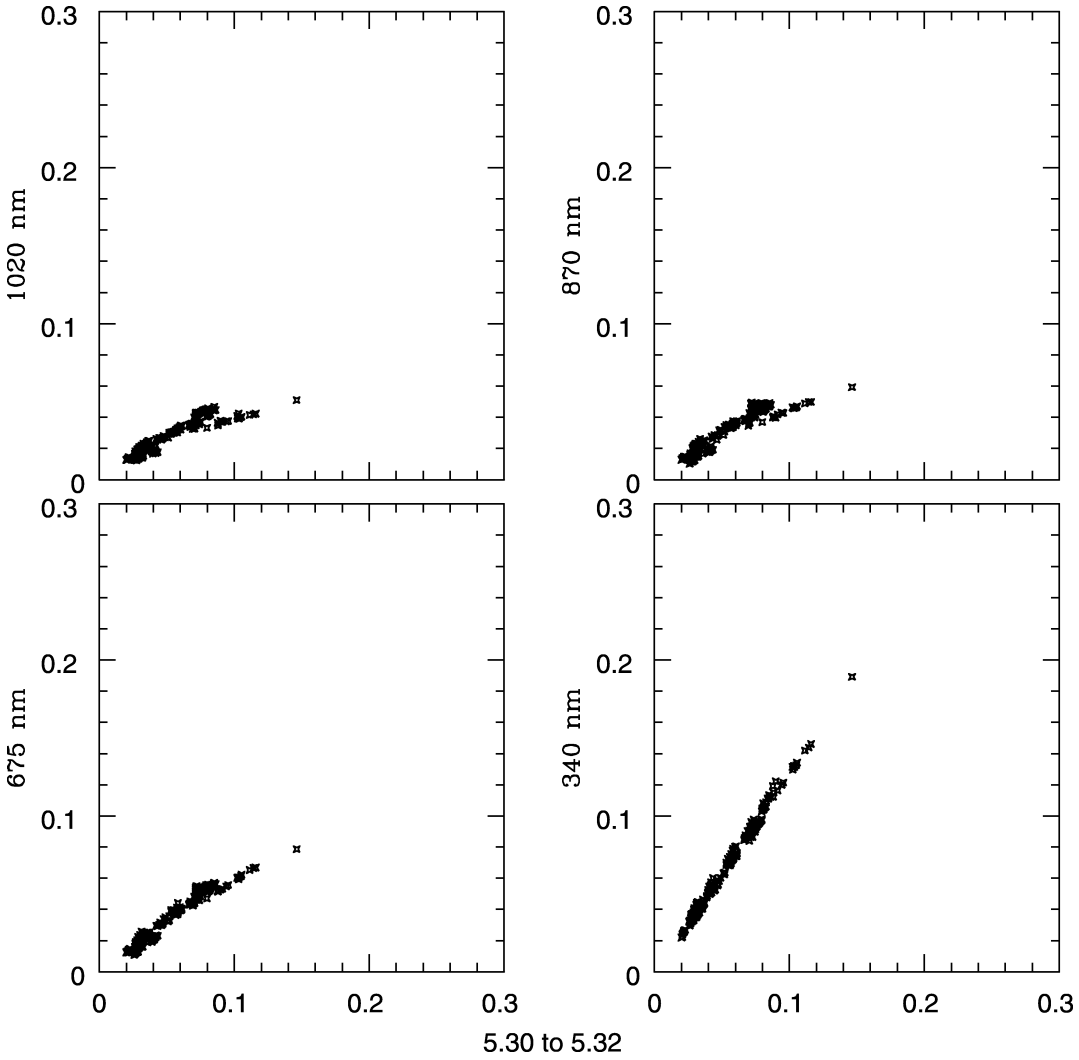

FIG. 5.—Extinction excursion. Same asFig. 4, but for the period between 5.30 and 5.32 yr. This attenuation spike appears to be predominantly due to aerosols.

percent, we need only know the ozone content with a fractional precision of around 10%. Eck et al. (1998) state that a 50% change in ozone content would perturb the optical transmission by 0.0036, 0.0045, and 0.0063 at 340, 500, and 657 nm, respectively.

We expect, therefore, to be able to exploit data obtained from satellites to constrain nightly variations in attenuation due to ozone, verified by direct measurements of atmospheric throughput on and off the well-known spectral regions of ozone attenuation.

2.4.3. Water

Frogel (1998) presents evidence for variation of atmospheric attenuation due to water, measured in the IR, and shows month-to-month and longer term variability. Roosen & Angione (1977) show that surface humidity measurements only poorly correlate with the upper atmospheric water burden. Attempts (Bessell 1999) to make a statistical correction to spectra for the absorption due to water have significant residuals, compared to oxygen A and B bands, which is evidence for significant variability. The PanSTARRS filter set includes a *y* band that takes advantage of the enhanced red response of high-resistivity CCDs, and the break between the PanSTARRS *z* and *y* bands has been selected to avoid the large water absorption feature at 950 nm. Nevertheless, there are H_2O absorption features, as shown in Figure 1, that impact other spectral regions.

Figure 9 is a cumulative distribution of the measured water content in the atmosphere over a 10 yr period, from the AERONET station on Mauna Loa. The units used are centimeters of precipitable water. Figure 10 shows the temporal evolution of the water content over the same period shown for the aerosols in Figure 2.

Thomas-Osip et al. (2007) present an interesting comparison of measurements of atmospheric water content using both

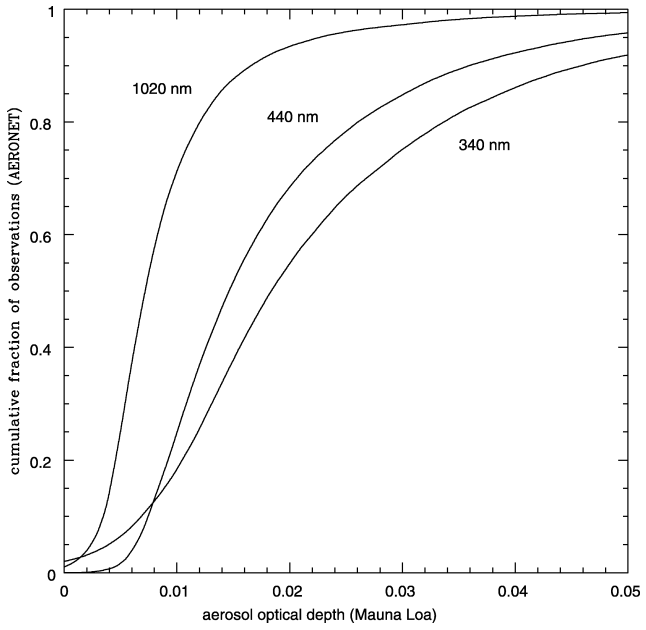

FIG. 6.—Aerosol optical depth statistics. Cumulative distributions of aerosol optical depth on Mauna Loa are shown from the AERONET observations over the period shown in Fig. 2.

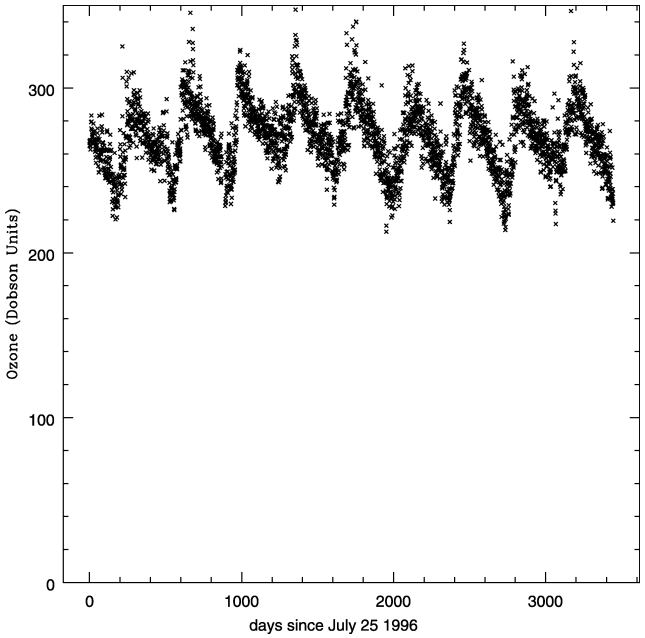

FIG. 8.—Ozone attenuation variability. This plot shows the evolution of the ozone content of the atmosphere vs. time above Hilo, HI, as measured by the *Earth Probe* TOMS satellite-borne instrument. The *y*-axis is in Dobson units. Each Dobson unit is equivalent to a thickness of 0.01 mm of ozone at STP. There is clear evidence of annual cyclic variation at the $\pm 25\%$ level about the mean value. Remote sensing data such as these can be used to determine the optical attenuation due to ozone without needing any ground-based measurements.

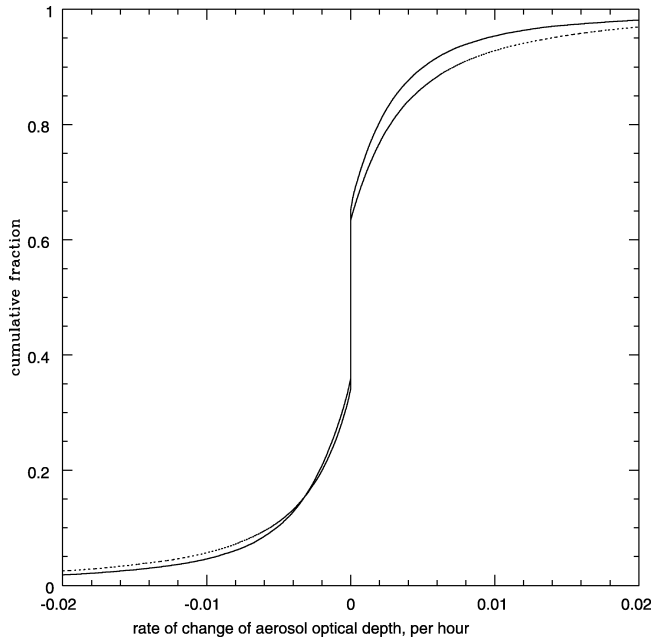

FIG. 7.—Variation statistics for aerosol optical depth. Cumulative distributions of aerosol optical depth changes (per hour) for the AERONET data on Mauna Loa are shown. The solid line corresponds to 1020 nm and the dashed line to 440 nm.

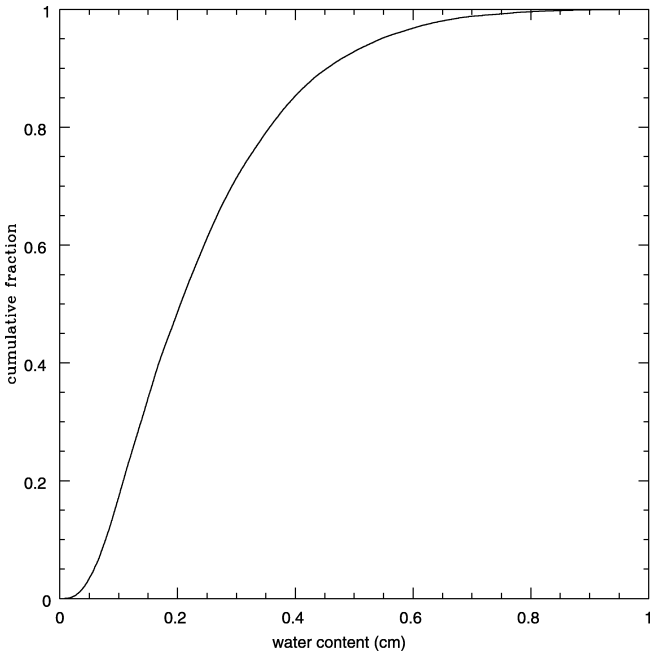

FIG. 9.—Cumulative distribution of precipitable water content (centimeters) above Mauna Loa, from the 12 yr AERONET data set.

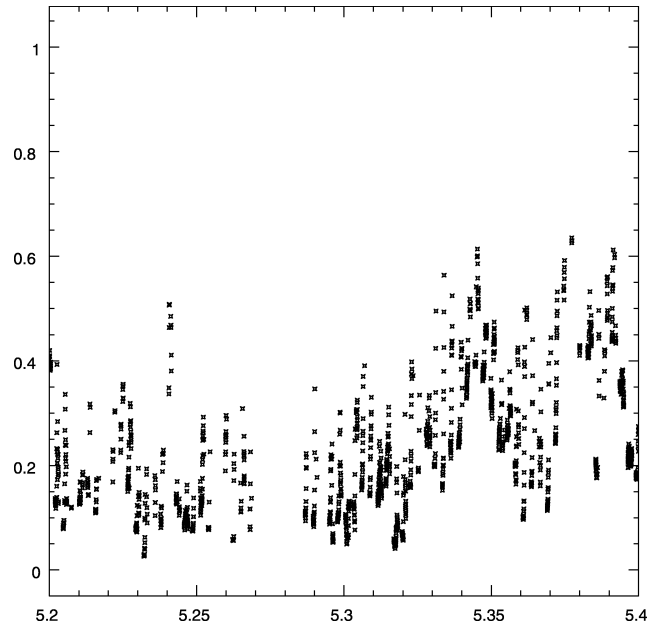

FIG. 10.—Time evolution of water content of the atmosphere at Mauna Loa. This plot of water content (in centimeters) vs. time covers the same interval as the plots in Fig. 3.

225 GHz radiometry and high-resolution optical spectroscopy. Their paper contains a valuable review of the physics of optical absorption by water vapor and demonstrates good agreement between the results obtained with these two techniques. They also show data with clear indications of short-term variability in atmospheric water, over the course of a night. The use of RF radiometry for the determination of water absorption in the optical clearly merits further consideration.

The evidence indicates that we should expect substantial temporal fluctuations in the optical absorption due to water, and this implies a potential azimuth dependence as well. We therefore conclude that optical attenuation due to water in the atmosphere is our second main challenge, with a complex behavior of both $\alpha_{\rm water}(\lambda)$ and $T_{\rm water}(\lambda,\hat{z},t)$.

2.4.4. Clouds

Water droplets and ice crystals also attenuate the transmission of optical radiation through the atmosphere. The standard assumption is that these objects that make up clouds are sufficiently larger than the wavelengths in question that the scattering is wavelength independent, so clouds are "gray" scatterers. Everett & Howell (2001) achieved Poisson-limited performance in differential photometry through high cirrus, lending credence to the idea that clouds are gray absorbers. Clouds can be detected through their emission (e.g., with a camera operating in the 10 μm band), by optical attenuation (through their effect on survey photometry), or in reflection (using LIDAR; see BenZvi et al. 2007a).

A thorough examination by Ivezić et al. (2007) of drift-scanned SDSS data from repeated imaging of stripe 82 has also shown little dependence of photometric residuals with color, even through many magnitudes of extinction from clouds, and even when comparing u- and z-band fluxes. These authors place an upper limit of 0.02 mag of zero-point uncertainty for photometry obtained through 1 mag of extinction from clouds. It is important to distinguish "astronomical point source" transmission through clouds, which we take to be the unscattered component, from the net radiation transfer of flux from the Sun, as described in Kylling et al. (1997).

One might imagine that a survey would need at least one visit to each field under highly photometric conditions in order to achieve a uniform all-sky zero point in each passband. The SDSS experience suggests that the location of the stellar locus, in color-color space, might be used to make zero-point corrections for those bands that were imaged through clouds. This of course assumes that the stellar locus has no dependence on Galactic coordinates.

PanSTARRS is planning to use a modest-aperture photometric monitor that places the entire survey field of view onto a single CCD array. This imager will be used to monitor the flux from Tycho catalog stars in the field (Magnier 2007). Using these objects as flux references will allow for the detection of even small amounts of gray extinction, and scatter in the flux differences across the field will be indicative of variable cloud across the field of view.

Contrails from aircraft are a nuisance that the astronomical community has not really faced up to. These could in principle be detectable by searching for residuals in the stellar locus that are linear across a frame, and excising or correcting the afflicted data. While we are not aware of any project that has done this, it should be straightforward. An approach akin to the excision of satellite tracks could be implemented, for example, based on photometric residuals that lie along a common line in an image.

3. THE ANGULAR AND TEMPORAL CORRELATION FUNCTIONS OF ATMOSPHERIC TRANSMISSION

The different contributions to atmospheric optical attenuation have different expected azimuth, zenith angle, and time dependencies. Short-term (during the night) time variability must necessarily be accompanied by variation in the azimuth and zenith angle dependence. The converse is not necessarily true, as we can imagine nonaxisymmetric configurations of the atmosphere that are stable over a night.

Anderson et al. (2003) have published the two-point correlation functions in space and time for aerosol scattering, but their data were not necessarily representative of an astronomical site. Nevertheless, they show evidence for the aerosol scattering component being highly correlated (correlation coefficient $r > 0.8$) over timescales of many hours and length scales of tens of kilometers.

We took the time-series AERONET data and determined the rate of change of aerosol optical depth at 1020 and 440 nm. Figure 7 shows the cumulative distribution of the rate of change

of the measured attenuation, in units of optical depth change per hour. It would appear that hourly measurements would have optical depth changes of under 0.01 hr^{-1} for more than 90% of the time, assuming that nighttime variation is similar to the daytime AERONET data set. Taking 10 m s^{-1} as a typical wind speed at the typical aerosol height of $z = 4$ km, in 1 hr the atmosphere will have translated by 36 km. This implies that the aerosol burden is correlated over at least this angular scale. We can therefore be optimistic that the aerosol attenuation will be correlated across the sky, for 1 hr at a time.

A similar analysis for the rate of change of water is shown in Figure 11. This appears more demanding. The water column can change by 10% in less than 1 hr, implying an azimuth variation as well. Figure 10 clearly shows as much as a factor of 4 variation in water content of the atmosphere at Mauna Loa. Since we would expect the optical depth due to water to scale as the square root of the water content in the air, this implies a factor of 2 fluctuation in optical attenuation due to water. Referring back to Table 1, we note that water absorption accounts for 3% and 5% attenuation in the z and y bands, respectively, at the zenith. This in turn implies that we should expect 1%–2% variations in zero point in these bands due to atmospheric water content variation. This effect will of course increase with zenith angle.

An important contribution by Ivezić et al. (2007) is their measurement of the structure function of clouds. These authors state that the zero-point offset between two regions is proportional to both the angular separation θ and the cloud's extinction A, with $\Delta m \sim (0.02–0.10)A(\theta/1°)$. This implies that local relative photometry can be extracted through clouds over surprisingly large areas, in agreement with the results from Everett & Howell (2001).

3.1. The Implications of a Wide Field of View, and Aperture Considerations

Much of the methodology currently used for correcting for atmospheric extinction is carried forward from the era of single-pixel detectors, but a distinguishing feature of the next generation of sky surveys is their wide field of view and gigapixel CCD arrays. The PanSTARRS and LSST imagers will span 3.0° and 3.5°, respectively, from corner to corner. Even at a modest zenith angle of 60°, the span in air mass across the LSST imager will range from 1.9 to 2.1! Taking the extinction values from Table 2, the *differential* extinction across the field will be 0.10, 0.04, 0.02, and 0.01 mag in u, g, r, i, and z, from this effect alone, at $\chi = 2$ air masses.

Our measurements are under the influence of attenuation processes that exhibit different air-mass dependences, so we cannot simply assign a single effective atmospheric transmission curve to each survey image, but instead we should calculate what amounts to a wavelength-dependent illumination correction across the field of view.

The atmospheric column traversed by the light from different objects depends on their separation and on the aperture of the telescope. Using the same arithmetic that applies to multiconjugate adaptive optics, the beams from two sources separated by an angle θ traverse distinct regions of the upper atmosphere only above a height $h > D/\sin\theta$, where D is the telescope aperture. This means that for LSST, with $D = 8.5$ m, the atmospheric transmission below $h = 15$ km is "common mode" for objects closer than 1′ on the sky. Aerosol attenuation arising from a static layer at $z \sim 4$ km would be common over a focal plane region spanning 3′ on LSST and 0.6′ for PanSTARRS. Local atmospheric perturbations in the first few hundred meters above the observatory are common mode across the entire LSST field. The dynamics of the atmosphere greatly suppress possible variation across the field of view, however. A 10 m s^{-1} wind will drag hundreds of meters of atmosphere across the telescope aperture over a typical survey exposure time of 15 or 30 s. This serves to homogenize the time-averaged atmospheric profile through which the system is imaging, at least in one dimension, across the entire field of view.

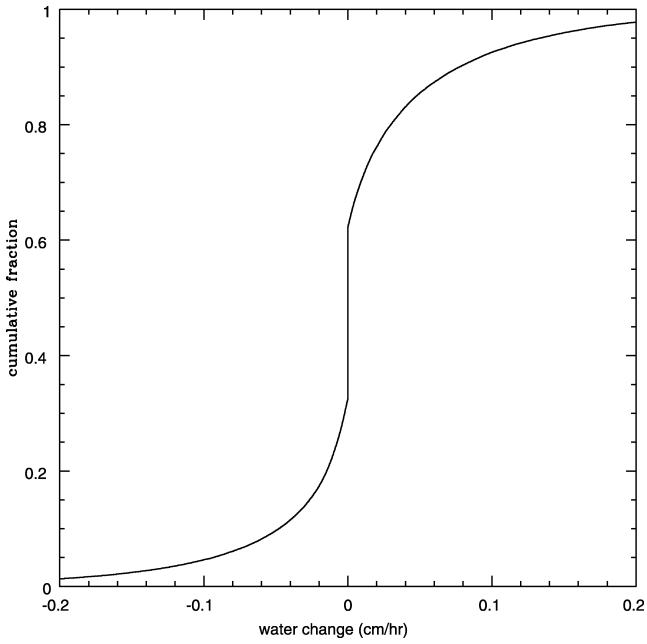

FIG. 11.—Cumulative plot of rate of change of AERONET's derived precipitable water content (centimeters per hour). For a typical value of 0.2 cm this implies that measurements more frequently than hourly are required to track 10% changes with confidence.

3.2. Measurement Priorities

Based on the above considerations, we can expect the Rayleigh and O_2 components of atmospheric transmission to be well behaved, with minimal variation from night to night and little azimuth dependence. The spectral shape of these mechanisms is also essentially time independent. The aerosol term, on the other hand, clearly shows evidence for temporal variation and spectral evolution and is difficult to measure. Water absorption has a fixed spectral profile, but its strength is highly

time variable. Clouds are gray absorbers at the 1% level, with significant temporal variation. Ozone absorption is time variable but can be measured from satellites. Our priorities are therefore the determination of aerosol scattering and absorption due to water molecules.

4. SPECTROSCOPIC MEASUREMENTS OF ATMOSPHERIC TRANSMISSION

There is a long tradition in astronomy of using spectrophotometry to determine the spectral energy distribution of celestial sources of interest. An integral part of the analysis of these data is to compensate for atmospheric attenuation. This naturally provides an opportunity to determine the wavelength dependence of atmospheric transmission, within the spectral resolution limitations of the apparatus. Bessell (1999) devised a technique to disentangle the spectral structure of the atmosphere from that of the celestial source. Stritzinger et al. (2005) used a combination of their spectroscopic observations and stellar models to produce a tabulation of extinction values versus wavelength, derived from their measurements of spectrophotometric standard stars. We caution, however, that their tabulated extinction values do not include molecular absorption effects. We can consider the smooth extinction data of Stritzinger et al. (2005; their Fig. 2) to be a good complement to the high spectral resolution absorption atlas of Hinkle et al. (2003).

In principle, high-precision spectrophotometry seems like the ideal way to measure the atmospheric attenuation profile. Measuring the Rayleigh, aerosol, and ozone attenuation does not require much spectral resolution (on the order of $\sim$1 nm) but does benefit from a large spectral range (300 nm to 1 μm) and requires high-precision spectrophotometry. The strength of the molecular absorption features can be expressed in equivalent widths (as commonly done among stellar spectroscopists), and since this is a spectrally local differential measurement, broadband flux precision and knowledge of the source spectrum are less of a concern.

One major advantage of the spectroscopic approach is that the measurements at all wavelengths are made simultaneously. This helps distinguish spatial from temporal variation in transmission.

There are two possible approaches to using spectroscopy for the determination of atmospheric extinction. If the spectrum of the source and the wavelength dependence of the instrumental sensitivity are well known, a single measurement of the spectrum of the source suffices to determine the atmospheric attenuation versus wavelength. On the other hand, measurements obtained at a diversity of air masses can be used to distinguish between the air mass-independent aspects (source spectrum and instrumental throughput) and the air mass–dependent atmospheric attenuation, liberating us from having to know the source spectrum. This second approach, of course, is susceptible to systematic errors due to any time dependence of the atmospheric extinction.

Drawbacks to the spectroscopic approach include the loss of signal-to-noise ratio, compared to the imaging techniques described below, due to dispersion. There are also nontrivial instrumental challenges. Grating dispersion elements have a large variation in throughput with wavelength, and maintaining a high signal-to-noise ratio across a wide spectral range is difficult due to limited CCD response at the limits of the targeted wavelength range. Prisms have higher dispersion in the blue than the red, which is the inverse of what we would like to have, although this is in part compensated by the loose constraint on spectral resolution.

A slitless spectrograph is essential for high-precision measurements in the blue at high air mass, but guiding errors can produce a systematic offset between the wavelength solution from arc lamps and the actual spectrum of the object. Nevertheless, the object spectrum itself can be used to determine a wavelength solution through identification of lines commonly found in stellar spectra (such as the Balmer series of hydrogen).

Extracting information about the distinct attenuation processes described above invariably involves comparing the fluxes in certain spectral regions and (for the absorption lines) determining equivalent widths. This means that the spectrometer is essentially being used as a simultaneous narrowband imager.

We have begun observing campaigns at Haleakala and CTIO designed to address these issues. The first steps have focused on assessing our ability to detect the signatures of the elements of atmospheric extinction in modest-resolution ($R \sim 400$) stellar spectra. Multiple stars are observed as they progress across the night sky. Spectral features whose strengths vary with air mass are extracted by fitting to templates of atmospheric extinction computed with models. By use of appropriate patterns of stars on the sky one can attempt to disentangle the spatial and temporal characteristics of the major contributors to extinction. Results from these studies will be subjects of future papers.

We carried out spectroscopy of a variety of standard stars of spectral class O–F at the Hawaii 2.2 m on Mauna Kea, using the SNIFS spectrograph (Lantz et al. 2004), and on the CTIO 1.5 m with their Ritchey-Chrétien spectrograph. We will report on our results in subsequent publications, but as described in § 7.1 our preliminary reductions illustrate the diagnostic power of spectroscopy in conjunction with transmission models for determining the air-mass dependence of atmospheric attenuation.

5. PHOTOMETRIC MEASUREMENTS OF ATMOSPHERIC TRANSMISSION

To measure extinction using imaging systems, astronomers have traditionally used the same broadband imaging system used for their program targets to observe standard stars. This automatically avoids the "color terms" required when transforming between photometry from different telescopes, cameras, or filters. If a set of comparison stars with spectra identical to the program objects can be found in the same field, this can potentially deliver high photometric precision. For Pan-

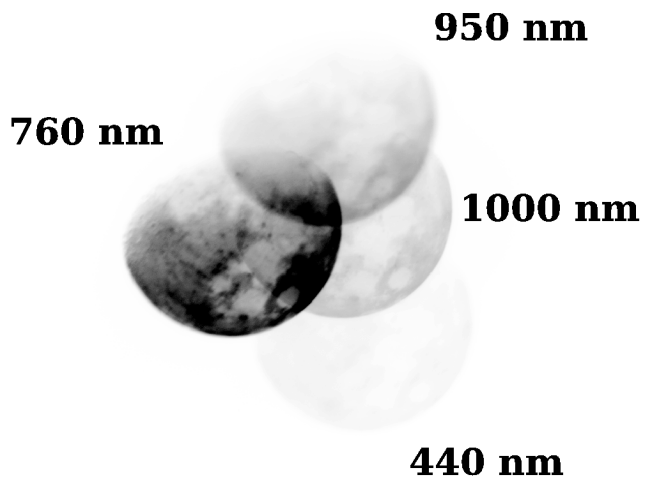

FIG. 12.—Image of the moon obtained simultaneously in four passbands, as part of our development of a simultaneous multiband imaging instrument designed to measure atmospheric transmission in real time. Images of a point source would be well separated, and the flux differences can be used to deduce attenuation.

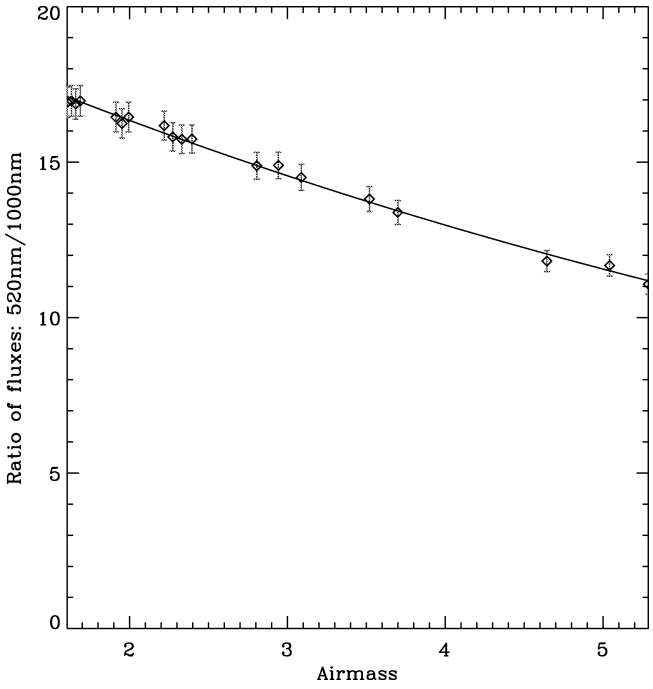

FIG. 13.—Aerosol attenuation data from simultaneous multiband imaging. This plot shows preliminary relative attenuation results that we obtained using the multiband imager, from CTIO. The vertical axis is the ratio of transmission at 440 nm to that at 1000 nm, plotted vs. air mass. The two fluxes were obtained simultaneously using the instrument described in the text. We consider this a promising technique to determine attenuation from both aerosol and molecular processes.

STARRS and LSST this approach is impractical, due to the time needed to change filters.

A number of programs have been undertaken to characterize the behavior of atmospheric transmission. At the risk of oversimplifying, the astronomical community has turned their instrumentation to this task, typically using standard astronomical passbands. The atmospheric sciences community, on the other hand, has been acquiring data with filter sets that are optimized for understanding the properties of the atmosphere. Most of their imaging is done in the daytime, however.

Schuster et al. (2002) describe a campaign of attenuation measurements using 13 narrowband filters that span 330 nm $< \lambda <$ 630 nm. However, these filters were chosen for measuring the properties of stars, not Earth's atmosphere.

5.1. A Simultaneous Multiband Stellar Photometer to Measure Attenuation

We have built and are now testing a dedicated, simultaneous multinarrowband imaging photometer (F. W. High et al. 2007, in preparation). The system uses a mask at the optical aperture, onto which wedge prisms and narrowband filters are mounted, in front of a fast camera lens. We put these on a commercial deep-depletion CCD camera (Pixis 1024BR, from Princeton Instruments) to achieve the same QE that we expect from PanSTARRS and LSST, and take pictures of bright stars. A prism wedge offsets the angle of light rays from a given star just in front of the aperture, resulting in an offset but still localized stellar image at the focal plane. By orienting each wedge differently and filtering their light independently, we produce an array of PSFs from a given star at different wavelengths in a single exposure.

The filter set is akin to that used for daytime solar photometers that are used to characterize the atmosphere. We chose the central wavelength of one filter to coincide with the main water absorption feature at 950 nm and another just off the feature at 1000 nm. Another filter coincides with the narrow oxygen absorption band at 760 nm, and the other three are positioned where the Rayleigh/aerosol scattering dominates. All our filters have FWHM of 10 nm. This filter set allows us to probe the main, narrow absorption bands and the Rayleigh/aerosol scattering components. Using a single common shutter makes this a clean differential measurement.

A test image from our simultaneous multiband imager is shown in Figure 12, and a representative profile of optical transmission versus air mass is presented in Figure 13. Such an apparatus is compact and largely made from commercially available parts. During operation, it leaves the scientific program uninterrupted. The data would later enter directly and quantitatively into the atmospheric attenuation model during analysis. It is therefore an interesting potential alternative to the traditional sequential broadband imaging methods.

6. ACTIVE INTERROGATION OF THE ATMOSPHERE: LIDAR

The atmospheric science community has long used LIDAR to probe the properties of the atmosphere. The book by Mea-

sures (1984) is a comprehensive reference for this technique. A LIDAR system sends pulses of light up through the atmosphere and measures the intensity of backscattered light as a function of time. The difference in light-travel time to different altitudes provides a method for probing the vertical structure of the atmosphere.

Light pulses emitted into the atmosphere can be scattered elastically or inelastically. The latter process results in a wavelength shift in the scattered light after internal degrees of freedom are excited in the scattering particles. Inelastic scattering has a smaller cross section, so the detection of these events requires some combination of a more intense light source and a detector with a larger aperture than is necessary to measure elastic scattering. The benefit of measuring the inelastic channel is the ability to isolate the type of scattering particle by measuring only the light shifted by specific wavelengths corresponding to quantum mechanical transitions for a chosen molecule such as N_2 or O_2, for which the vertical density profiles are well known. These constraints on the probability of scattering from the inelastic channel allow for direct measurement of round-trip extinction.

LIDAR systems exploiting both the elastic and inelastic channels have been used for decades to study atmospheric properties. Melfi (1972) gives an overview of inelastic (Raman) techniques, and Vaughan et al. (1993) describe using inelastic scattering to obtain precise temperature profiles in the atmosphere. Zimmer et al. (2007) and Dawsey et al. (2006) have described their program of developing an eye-safe elastic-channel single-wavelength LIDAR system for the determination of atmospheric extinction of astronomical sources, and we look forward to results from this system once it is deployed. The use of multiple elastic-scattering LIDAR systems to carry out what amounts to a tomographic measurement of aerosols above an observatory is described in BenZvi et al. (2007a).

A high-power, tunable laser could be used to measure inelastic scattering and map atmospheric transmission over the wavelengths of interest. Measurements at multiple wavelengths can determine relative atmospheric transmission without any need for information about the molecular density profile, which is usually taken from models such as the US Standard Atmosphere (COESA 1976) for absolute single-wavelength measurements. We note that the transmission of the atmosphere at 1.064 μm is very high, and this is a natural reference point, since high-intensity Nd:YAG lasers emit at this wavelength.

A simultaneous multiband LIDAR system could detect both the elastic and inelastic return signals. Using a tunable laser would allow us to measure on- and off-band regions near the water absorption feature, thereby measuring the strength of that feature. The LIDAR system can be aligned with the main survey system and can take data during the readout and slew of the survey instrument.

The ability to map out the vertical profile of attenuation might provide a way to distinguish between attenuation processes that are spectrally coincident, such as aerosols (concentrated in the lower regions of the atmosphere) and ozone (concentrated in the lower stratosphere). In addition, even thin clouds at high altitudes can be detected as an overdensity of scattering particles. This added height dimension could contribute to atmospheric models discussed in the next section.

LIDAR is a mature technique that is commonly used in the atmospheric sciences but has not yet been applied to the astronomical extinction problem. The use of high-power lasers at astronomical observatories does pose issues of safety, as well as interference with photometric measurements at sites with multiple telescopes. However, adaptive optics systems already in place use similar devices, which indicates that such problems are surmountable. We suspect that the narrowband laser light from a nanosecond pulse tunable laser (with $\delta\lambda \sim 0.5$ nm) is probably better suited to measuring the aerosol scattering rather than water vapor absorption. A faster laser pulse would be correspondingly broader, of course.

7. MODELING THE TRANSMISSION OF THE ATMOSPHERE: MODTRAN

Sophisticated radiative transfer codes exist to model the transmission properties of Earth's atmosphere. Here we discuss MODTRAN, the moderate spectral resolution atmospheric transmittance code developed by the US Air Force Research Lab (Anderson et al. 2001). MODTRAN produces a transmission function, from optical to infrared, for arbitrary lines of sight through the atmosphere. The code can be used with an input atmospheric profile, in full spherical refractive geometry, to decompose the integrated air mass into the altitude-dependent opacity along the line of sight. The calculations are based on spectroscopic band models and provide a maximum resolution of 2 cm^{-1}. The band model approach is fast but is limited to local thermodynamic equilibrium (LTE) conditions. Non-LTE effects can be neglected in the lower atmosphere, below 50 km, but may become important for species found in the upper atmosphere. The molecular species modeled by MODTRAN are derived from the HITRAN database (Rothman et al. 2005) and include H_2O, CO_2, O_3, N_2O, CO, CH_4, HNO_3, NO, NO_2, SO_2, O_2, N_2, and NH_3. As noted by Bailey et al. (2007) and Adelman et al. (1996) the HITRAN database is not complete and it may be useful to augment the line list with updated laboratory or observational results. Aerosol scattering is modeled in discrete layers through the atmosphere. Generic troposphere models (desert, rural, urban, maritime) are available, as well as water vapor contributions from clouds. User-defined data may be substituted to extend the models to particular conditions of interest.

MODTRAN is also capable of producing an emission calculation to model sky glow. However, it is restricted to the thermal contributions. The important night-sky emission lines are produced deep in the non-LTE regime hundreds of kilometers up in the atmosphere and are not modeled.

7.1. Blending Measurements with Models

In our preliminary study, we have adapted MODTRAN for the atmospheric conditions of Mauna Kea Observatories. This procedure will be extended to PS1 on Haleakala and, in principle, can be used to produce an atmospheric model appropriate for any observatory. The Mauna Kea Weather Center provides real-time temperature, pressure, and humidity measurements from the ground, as well as daily balloon radiosonde data to map the altitude profile. We have used these measured pressure and temperature profiles to generate an input atmosphere definition for MODTRAN. The Weather Center also provides the water vapor profile, which can be incorporated into the model atmosphere directly. To derive the concentrations of other molecular species, we simply scale the concentrations in the generic US Standard Atmosphere by the pressure and temperature.

The atmospheric transmission models hide hundreds of free parameters. We have explored the minimum set necessary to fit the measured atmospheric features in measured stellar spectra with MODTRAN models and find that, with appropriate model atmosphere profiles, we can fit observations by scaling only the water vapor content.

Figure 14 shows a measured O star spectrum from our Mauna Kea data set, overplotted with a MODTRAN model. The spectrum has been flattened and normalized to isolate the line absorption features. The primary absorption bands of interest in the optical are the oxygen line at 760 nm and the water band at 950 nm. We tune the MODTRAN output to these features by first fixing the line of sight to match the observation and then scaling the oxygen and water vapor concentrations to match the absorption depths. The water vapor is the dominant absorber in the MODTRAN model, and we can put strong constraints on it through the fit. It is less sensitive to the oxygen concentration. Thus, through joint spectroscopic measurements and modeling, the temporal and spatial variations in water vapor can be effectively tracked.

Atmospheric transmission models can be integrated into an observatory using measurements from a dedicated instrument to monitor key absorption features. As discussed, a simple system could consist of a dedicated imaging camera with narrowband filters centered on strong atmospheric absorption bands. The camera would collect atmospheric transmission data in synchrony with the survey telescope operations and provide constraints on oxygen and water vapor concentrations, as well as aerosol scattering. These measurements could then be fit by an atmospheric modeling code, such as MODTRAN, to produce a full, high-resolution transmission function representing a particular line of sight and time period.

8. SUMMARY AND NEXT STEPS

This paper addresses the goal of achieving precise relative photometry over the course of next-generation "all-sky" imaging surveys such as PanSTARRS and LSST. Calibrations of absolute scales may also be possible, but the scientific goals

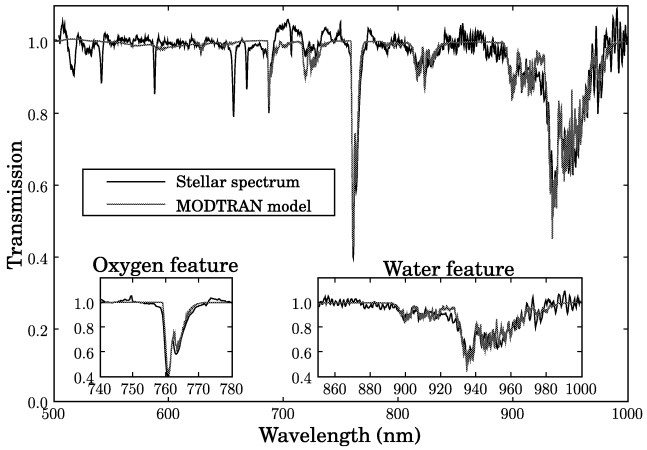

FIG. 14.—Spectrum that we obtained on the UH 88 inch telescope, normalized to show absorption features. The inset panels show the comparison between the observed spectrum and MODTRAN output, for the parameters shown. We intend to pursue the idea of combining observations and models to determine the optical transmission function of the atmosphere.[*See the electronic edition of PASP for a color version of this figure.*]

for these future surveys stress uniformity of the photometry across large scales on the sky, and the identification of time-dependent celestial phenomena.

Our thesis is that significant improvement in photometric measurement, perhaps even to the millimagnitude level of relative precision, can be enabled by direct measurement of atmospheric throughput. Several techniques for making such measurements are suggested, but all rely on identification of a relatively small number of contributors to atmospheric extinction—the final four. Each of these contributors leaves characteristic signatures in transmitted spectra. It is the challenge of our approach to show how to detect and quantify these signatures with sufficient temporal and spatial resolution to allow precise relative photometric measurements to be made.

Molecular absorption is significant for only a few species (specifically ozone, oxygen, OH, and water vapor) and occurs at well-known and characteristic wavelengths. Water vapor column heights vary substantially with atmospheric conditions, but optical depths of remaining molecular constituents are simply given by barometric pressure. The theory of Rayleigh-Carbannes molecular scattering is well developed, and the process presents a strong and stable λ^4 signature that is easily recognized. Measurement of aerosol scattering is considerably more troublesome.

We anticipate that the variability of both the aerosol content of the atmosphere and the water content will present the dominant atmospheric limitation to precision photometry from next-generation surveys. This suggests that instrumentation development focus on these two concerns.

Our analysis leads to some thoughts on future research. First, we conclude that, while it may be possible to "tune up" tech-

niques and algorithms with parasitic use of existing data, it will be necessary to carry out dedicated measurements to test the ultimate capability of any of these to meet our goals. This conclusion is not surprising, since what we are trying to do has not been done before; i.e., no existing data set has met the goals of these next-generation surveys.

In follow-on campaigns it will be most useful to carry out tests with simultaneous spectroscopic measurements of stars with photometric measurements of a number of standard targets. While these measurements need not be carried out over the scales of future surveys, they will need to be made with care and dedication if it is to be shown that survey-wide millimagnitude photometry is possible.

We thank Justin Albert, Tim Axelrod, James Battat, Yorke Brown, Kelly Chance, Chuck Claver, Kem Cook, Doug Finkbeiner, Jim Gunn, Žjelko Ivezić, John McGraw, Gene Magnier, Eli Margalith, David Schlegel, Nick Suntzeff, and Doug Welch for useful conversations and input. We are very grateful for the efforts of the AERONET consortium, and Brent Holben in particular, both for the establishment and operation of the aerosol monitoring site on Mauna Loa and for making the AERONET data readily available on the Web. We have also used results from the Total Ozone Mapping Spectrometer (TOMS) on the *Earth Probe* satellite, and we are grateful to the team that built and operated this instrument. We thank the LSST Corporation, Harvard University, the Department of Energy Office of Science, and the US Air Force Office of Scientific Research for their support of this work. The LSST design and development activity is supported by the National Science Foundation under Scientific Program Order No. 9 (AST 05-51161) through Cooperative Agreement AST 01-32798. Additional support was provided through the NSF award to the ESSENCE supernova cosmology project, through AST 06-07485. Portions of this work were performed in part under Department of Energy contracts DE-AC02-76SF00515, DE-AC02-98CH10886, DE-FG02-91ER40677, and W-7405-Eng-48. Additional funding comes from private donations, in-kind support at Department of Energy laboratories, and other LSSTC Institutional Members.

REFERENCES

Adelman, S. J., Gulliver, A. F., & Holmgren, D. E. 1996, in ASP Conf. Ser. 108, Model Atmospheres and Spectrum Synthesis, ed. S. J. Adelman, F. Kupka, & W. W. Weiss (San Francisco: ASP), 293
Albert, J., et al. 2006, preprint
Anderson, G. P., et al. 2001, Proc. SPIE, 4381, 455
Anderson, T. L., et al. 2003, J. Atmos. Sci., 60, 119
Bailey, J., Simpson, A., & Crisp, D. 2007, PASP, 119, 228
BenZvi, S., et al. 2007a, in Proc. 30th Int. Cosmic Ray Conf. (Merida), in press (arXiv: 0706.1710)
BenZvi, S. Y., et al. 2007b, Nucl. Instrum. Methods A, 574, 171
Bessell, M. 1999, PASP, 111, 1426
Burke, D., et al. 2006, Proc. SPIE, 6267, 38
Committee on Extension to the Standard Atmosphere. 1976, US Standard Atmosphere (Washington: GPO)
Dawsey, M., Gimmestad, G., Roberts, D., McGraw, J., Zimmer, P., & Fitch, J. 2006, Proc. SPIE, 6270, 47
de Vaucouleurs, G., & Angione, R. J. 1973, PASP, 86, 104
Eck, T. F., et al. 1998, J. Geophys. Res., 103, 31865
Everett, M. E., & Howell, S. B. 2001, PASP, 113, 1428
Frogel, J. 1998, PASP, 110, 200
Hadrava, P. 2006, A&A, 448, 1149
Hansen, J. E., & Travis, L. D. 1974, Space Sci. Rev., 16, 527
Hartman, J. D., et al. 2005, AJ, 130, 2241
Hinkle, K. H., Wallace, L., & Livingston, W. 2003, BAAS, 35, 1260
Holben, B. N., et al. 2001, J. Geophys. Res., 106, 12067
Ivezić, Ž., et al. 2007, AJ, submitted (astro-ph/0703157)
Jaross, G., et al. 2003, AGU Fall Meeting, Abstr. A21D-0993
Kaiser, N., et al. 2002, Proc. SPIE, 4836, 154
Krisciunas, K., et al. 1987, PASP, 99, 887
Kurucz, R. 1993, Kurucz CD-ROM 13, ATLAS9 Stellar Atmosphere Programs and 2 km/s Grid (Cambridge: SAO)
Kylling, A., Albold, A., & Seckmeyer, G. 1997, Geophys. Res. Lett., 24, 397
Lantz, B., et al. 2004, Proc. SPIE, 5249, 146
Magnier, E. 2007, in ASP Conf. Ser. 364, The Future of Photometric, Spectrophotometric and Polarimetric Standardization, ed. C. Sterken (San Francisco: ASP), 153
Measures, R. 1984, Laser Remote Sensing (New York: Wiley)
Melfi, S. H. 1972, Appl. Opt., 11, 1605
Miknaitis, G., et al. 2007, ApJ, 666, 674
Padmanabhan, N., et al. 2007, ApJ, submitted (astro-ph/0703454)
Pakstiene, E. 2001, Baltic Astron., 10, 651
Rayleigh, Lord. 1899, Philos. Mag., 47, 375
Reimann, H.-G., et al. 1992, A&A, 265, 360
Roosen, R. G., & Angione, R. J. 1977, PASP, 89, 814
Rothman, L. S., et al. 2005, J. Quant. Spectrosc. Radiat. Transfer, 96, 139
Schuster, W. J., Parrao, L., & Guichard, J. 2002, J. Astron. Data, 8, 2
Sinyuk, A., et al. 2007, Remote Sensing of Environment, 107, 90
Stritzinger, M., et al. 2005, PASP, 117, 810
Stubbs, C., & Tonry, J. 2006, ApJ, 646, 1436
Stubbs, C. W., et al. 2007, in ASP Conf. Ser. 364, The Future of Photometric, Spectrophotometric and Polarimetric Standardization, ed. C. Sterken (San Francisco: ASP), 373
Thomas-Osip, J., McWilliam, A., Phillips, M. M., Morrell, N., Thompson, I., Folkers, T., Adams, F. C., & Lopez-Morales, M. 2007, PASP, 119, 697
Tonry, J. L., et al. 2005, PASP, 117, 281
Tucker, D. L., et al. 2006, Astron. Nachr., 327, 821
Vaughan, G., et al. 1993, Appl. Opt., 32, 2758
Wade, R. A., & Horne, K. 1988, ApJ, 324, 411
Young, A. T., et al. 1991, PASP, 103, 221
Zimmer, P., et al. 2007, BAAS, 38, 1109